Document made available under the Patent Cooperation Treaty (PCT)

International application number: PCT/US05/007652

International filing date: 10 March 2005 (10.03.2005)

Document type: Certified copy of priority document

Document details: Country/Office: US
Number: 60/570,690
Filing date: 13 May 2004 (13.05.2004)

Date of receipt at the International Bureau: 18 April 2005 (18.04.2005)

Remark: Priority document submitted or transmitted to the International Bureau in compliance with Rule 17.1(a) or (b)

World Intellectual Property Organization (WIPO) - Geneva, Switzerland
Organisation Mondiale de la Propriété Intellectuelle (OMPI) - Genève, Suisse

130844

THE UNITED STATES OF AMERICA

TO ALL TO WHOM THESE PRESENTS SHALL COME:

UNITED STATES DEPARTMENT OF COMMERCE

United States Patent and Trademark Office

April 01, 2005

THIS IS TO CERTIFY THAT ANNEXED HERETO IS A TRUE COPY FROM THE RECORDS OF THE UNITED STATES PATENT AND TRADEMARK OFFICE OF THOSE PAPERS OF THE BELOW IDENTIFIED PATENT APPLICATION THAT MET THE REQUIREMENTS TO BE GRANTED A FILING DATE.

APPLICATION NUMBER: ***60/570,690***
FILING DATE: ***May 13, 2004***
RELATED PCT APPLICATION NUMBER: ***PCT/US05/07652***

UNITED STATES PATENT AND TRADEMARK OFFICE
DEPARTMENT OF COMMERCE

Certified by

Jon W. Dudas

Under Secretary of Commerce
for Intellectual Property
and Director of the United States
Patent and Trademark Office

PTO/SB/16 (01-04) (modified)
Approved for use through 07/31/2006. OMB 0651-0032
U.S. Patent and Trademark Office; U.S. DEPARTMENT OF COMMERCE

PROVISIONAL APPLICATION FOR PATENT COVER SHEET

This is a request for filing a PROVISIONAL APPLICATION FOR PATENT under 37 CFR 1.53(c).

Express Mail Label No. ER 477497208 US

INVENTOR(S)

Given Name (first and middle [if any])	Family Name or Surname	Residence (City and either State or Foreign Country)
Vasilis	Ntziachristos	Charlestown, MA

Additional inventors are being named on the 1 *separately numbered sheets attached hereto*

TITLE OF THE INVENTION (500 characters max)

METHOD AND SYSTEM FOR OPTICAL TOMOGRAPHY USING FLUORESCENT PROTEINS

Direct all correspondence to: **CORRESPONDENCE ADDRESS**

☑ Customer Number: 022494

OR

☐ Firm or Individual Name	Kermit Robinson				
Address	Daly, Crowley & Mofford, LLP				
Address	275 Turnpike Street - Suite 101				
City	Canton	State	MA	Zip	02021-2354
Country	US	Telephone	781.401.9988	Fax	781.401.9966

ENCLOSED APPLICATION PARTS *(check all that apply)*

☑ Specification *Number of Pages* 46

☐ Assignment Papers (for an Application) Number of Pages

☐ Drawing(s) *Number of Sheets*

☐ CD(s), Number

☐ Application Data Sheet. See 37 CFR 1.76

☑ Other (specify) Return Postcard; Pat. Applic. Title Pg.

METHOD OF PAYMENT OF FILING FEES FOR THIS PROVISIONAL APPLICATION FOR PATENT

☑ Applicant claims small entity status. See 37 CFR 1.27.

☑ A check or money order is enclosed to cover the filing fees.

☑ The Director is herby authorized to charge filing fees or credit any overpayment to Deposit Account Number: 500845

☐ Payment by credit card. Form PTO-2038 is attached.

FILING FEE Amount ($): 80

The invention was made by an agency of the United States Government or under a contract with an agency of the United States Government.

☐ No.

☑ Yes, the name of the U.S. Government agency and the Government contract number are: NIH, R33-CA91807

Respectfully submitted,

SIGNATURE

Date May 13, 2004

REGISTRATION NO. 48,734 *(if appropriate)*

Docket Number: MGH-049PUSP

TYPED or PRINTED NAME Kermit Robinson

TELEPHONE 781.401.9988 ext. 24

USE ONLY FOR FILING A PROVISIONAL APPLICATION FOR PATENT

PROVISIONAL APPLICATION COVER SHEET
Additional Page

PTO/SB/16 (08-03)
Approved for use through 07/31/2006. OMB 0651-0032
U.S. Patent and Trademark Office; U.S. DEPARTMENT OF COMMERCE
Under the Paperwork Reduction Act of 1995, no persons are required to respond to a collection of information unless it displays a valid OMB control number.

Docket Number	MGH-049PUSP

INVENTOR(S)/APPLICANT(S)		
Given Name (first and middle [if any])	Family or Surname	Residence (City and either State or Foreign Country)
Jorge	Ripoll	Heraklion, Crete, Greece
Giannis	Zacharakis	Boston, MA

WARNING: Information on this form may become public. Credit card information should not be included on this form. Provide credit card information and authorization on PTO-2038.

PTO/SB/17 (10-03)
Approved for use through 07/31/2006. OMB 0651-0032
U.S. Patent and Trademark Office; U.S. DEPARTMENT OF COMMERCE

FEE TRANSMITTAL for FY 2004

Effective 10/01/2003. Patent fees are subject to annual revision.

☒ Applicant claims small entity status. See 37 CFR 1.27

TOTAL AMOUNT OF PAYMENT ($) **80**

Complete if Known	
Application Number	Not Yet Assigned
Filing Date	May 13, 2004
First Named Inventor	Vasilis Ntziachristos
Examiner Name	Not Yet Assigned
Art Unit	Not Yet Assigned
Attorney Docket No.	MGH-049PUSP

METHOD OF PAYMENT *(check all that apply)*

☒ Check ☐ Credit card ☐ Money Order ☐ Other ☐ None

☐ Deposit Account:

Deposit Account Number: 50-0845

Deposit Account Name: Daly, Crowley & Mofford, LLP

The Director is authorized to: *(check all that apply)*

☐ Charge fee(s) indicated below ☒ Credit any overpayments

☒ Charge any additional fee(s) or any underpayment of fee(s)

☐ Charge fee(s) indicated below, **except for the filing fee** to the above-identified deposit account.

FEE CALCULATION

1. BASIC FILING FEE

Large Entity Fee Code	Large Entity Fee ($)	Small Entity Fee Code	Small Entity Fee ($)	Fee Description	Fee Paid
1001	770	2001	385	Utility filing fee	
1002	340	2002	170	Design filing fee	
1003	530	2003	265	Plant filing fee	
1004	770	2004	385	Reissue filing fee	
1005	160	2005	80	Provisional filing fee	80

SUBTOTAL (1) ($) **80**

2. EXTRA CLAIM FEES FOR UTILITY AND REISSUE

	Extra Claims		Fee from below		Fee Paid
Total Claims	-20** =	0	X	=	0
Independent Claims	- 3** =	0	X	=	0
Multiple Dependent				=	

Large Entity Fee Code	Large Entity Fee ($)	Small Entity Fee Code	Small Entity Fee ($)	Fee Description
1202	18	2202	9	Claims in excess of 20
1201	86	2201	43	Independent claims in excess of 3
1203	290	2203	145	Multiple dependent claim, if not paid
1204	86	2204	43	** Reissue independent claims over original patent
1205	18	2205	9	** Reissue claims in excess of 20 and over original patent

SUBTOTAL (2) ($) **0**

***or number previously paid, if greater; For Reissues, see above*

FEE CALCULATION (continued)

3. ADDITIONAL FEES

Large Entity Fee Code	Large Entity Fee ($)	Small Entity Fee Code	Small Entity Fee ($)	Fee Description	Fee Paid
1051	130	2051	65	Surcharge - late filing fee or oath	
1052	50	2052	25	Surcharge - late provisional filing fee or cover sheet	
1053	130	1053	130	Non-English specification	
1812	2,520	1812	2,520	For filing a request for *ex parte* reexamination	
1804	920*	1804	920*	Requesting publication of SIR prior to Examiner action	
1805	1,840*	1805	1,840*	Requesting publication of SIR after Examiner action	
1251	110	2251	55	Extension for reply within first month	
1252	420	2252	210	Extension for reply within second month	
1253	950	2253	475	Extension for reply within third month	
1254	1,480	2254	740	Extension for reply within fourth month	
1255	2,010	2255	1,005	Extension for reply within fifth month	
1401	330	2401	165	Notice of Appeal	
1402	330	2402	165	Filing a brief in support of an appeal	
1403	290	2403	145	Request for oral hearing	
1451	1,510	1451	1,510	Petition to institute a public use proceeding	
1452	110	2452	55	Petition to revive - unavoidable	
1453	1,330	2453	665	Petition to revive - unintentional	
1501	1,330	2501	665	Utility issue fee (or reissue)	
1502	480	2502	240	Design issue fee	
1503	640	2503	320	Plant issue fee	
1460	130	1460	130	Petitions to the Commissioner	
1807	50	1807	50	Processing fee under 37 CFR 1.17(q)	
1806	180	1806	180	Submission of Information Disclosure Stmt	
8021	40	8021	40	Recording each patent assignment per property (times number of properties)	
1809	770	2809	385	Filing a submission after final rejection (37 CFR 1.129(a))	
1810	770	2810	385	For each additional invention to be examined (37 CFR 1.129(b))	
1801	770	2801	385	Request for Continued Examination (RCE)	
1802	900	1802	900	Request for expedited examination of a design application	

Other fee (specify) _____

*Reduced by Basic Filing Fee Paid **SUBTOTAL (3)** ($) **0**

SUBMITTED BY				(Complete *(if applicable)*)	
Name (Print/Type)	Kermit Robinson	*Registration No. (Attorney/Agent)*	48,734	*Telephone*	781.401.9988 ext. 24
Signature				*Date*	May 13, 2004

WARNING: Information on this form may become public. Credit card information should not be included on this form. Provide credit card information and authorization on PTO-2038.

If you need assistance in completing the form, call 1-800-PTO-9199 and select option 2.

UNITED STATES PROVISIONAL PATENT APPLICATION

of

Vasilis Ntziachristos
Jorge Ripoll
Giannis Zacharakis

for

METHOD AND SYSTEM FOR OPTICAL TOMOGRAPHY USING FLUORESCENT PROTEINS

DALY, CROWLEY & MOFFORD, LLP
275 Turnpike Street, Suite 101
Canton, MA 02021-2310
Telephone (781) 401-9988
Facsimile (781) 401-9966

Express Mail Label No.: ER 477497208 US

METHOD AND SYSTEM FOR OPTICAL TOMOGRAPHY USING FLUORESCENT PROTEINS

CROSS REFERENCE TO RELATED APPLICATIONS

Not Applicable.

STATEMENT REGARDING FEDERALLY SPONSORED RESEARCH

This invention was made with government support under Contract No. R33-CA91807 awarded by the National Institute of Health (NIH). The government has certain rights in the invention.

FIELD OF THE INVENTION

This invention relates generally to optical tomography and, more particularly, to a method and system for extracting quantitative, three-dimensional molecular and biological information from living subjects using fluorescent proteins.

BACKGROUND OF THE INVENTION

Fluorescence proteins (FPs) have become important reporter molecules for different biomedical applications. In some existing applications, engineered FPs are detected by epi-fluorescence, confocal (microscopy), or reflectance (whole animal) imaging. The latter has been shown to be useful in detecting and following tumors in vivo, particularly those implanted near the surface or in surgically exposed organs. However, reflectance imaging has inherent limitations, since the recorded images are a superposition of fluorescence signals from multiple depths, resulting in blurred images. Reflectance imaging does not retrieve depth information or allow absolute quantification of fluorescence activity. This is due in part to non-linear light attenuation and propagation in biological tissues, which limits the applicability of reflectance imaging to semi-quantitative imaging at depths of only a few millimeters.

Imaging optical signatures deeper in tissues requires the application of advanced light excitation and light detection apparatus and techniques and the use of tomographic principles

for combining data acquired at different projections. Advances in imaging with diffracting sources have resulted in several studies investigating tissue using intrinsically or extrinsically administered optical contrast. In particular, diffuse optical tomography (DOT) is a technique that can provide a tomographic image associated with a diffuse media in the presence of absorption and scattering in the diffuse media. For example, DOT has been applied toward cerebral hemodynamic imaging and imaging of breast tissue. One exemplary DOT method and system is described, for example, in international patent application PCT/US04/03229, by Vasilis Ntziashristos and Jorge Ripoll, entitled "Method and System for Free Space Optical Tomography of Diffuse Media," filed February 5, 2004, which application is assigned to the assignee of the present invention.

It has been shown that light with wavelengths in the near-infrared range can propagate through tissue for distances on the order of multiple centimeters because of low tissue absorption in the so-called "near-infrared window." The near-infrared (NIR) window has enabled the development of NIR fluorescence techniques to visualize specific biochemical events inside living subjects.

A variety of related methods for processing NIR fluorescence signals have also been developed, and their imaging capability has been demonstrated with simulated data and phantom measurements. The term "phantom," as used herein, is used to describe a manufactured object to be scanned, which can be used to test the scanning method and system. In particular, development of appropriate imaging systems has enabled the application of Fluorescence Molecular Tomography (FMT), a technique that resolves molecular signatures in deep tissues using NIR fluorescent probes or markers. FMT for in vivo three-dimensional imaging of enzymatic activity in deep-seated tumors has been demonstrated.

A common element to conventional NIR optical tomographic techniques developed for fluorescence reconstructions is that they assume propagation in a diffuse media with high scattering but with relatively low absorption provided by the NIR window. This assumption has allowed derivation of a "diffusion approximation" to the transport equation, providing an

effective tool for modeling NIR photon propagation in tissues. However, tomographic imaging using visible light is complicated by a relatively high absorption of visible light propagating in tissue, which results in significant attenuation. With high absorption, the diffusion approximation is not valid, particularly when imaging deep tissues.

More advanced solutions to the transport equation have been generated and applied to NIR optical tomography. The advanced solutions overcome the inadequacy of the above-mentioned diffusion approximation. However solutions to the transport equation are generally computationally expensive and become impractical for tomographic systems having large data sets. Also, transport-equation solutions have not been applied to tomographic imaging in media where high scattering and void regions co-exist, and no such solutions have been demonstrated for optical tomography using visible light.

Many conventional optical tomography systems use an optical scanning switch as part of a light source assembly in order to use a single light element to project at a variety of angles. It is known that the optical scanning switch generates energy losses. Furthermore, many optical tomography systems use a CCD camera at room temperature to collect light. It is known that a room temperature CCD camera exhibits a relatively high level of dark noise limiting the ability to generate optical tomography images.

SUMMARY OF THE INVENTION

A method and system for optical tomography using fluorescent proteins includes an efficient computational method for quantitative three-dimensional imaging using visible light, a laser providing visible light, which in combination with an optical scanning switch provides the visible light with proper characteristics, and a data collection apparatus adapted to receive corresponding visible light from highly absorbent media including visible fluorescent light emitted by the fluorescent proteins. In one particular embodiment, the optical scanning switch is replaced with an optical scanner, providing increased efficiency and increased controllability. In one particular embodiment, the data collection apparatus includes a cooled CCD camera having reduced dark noise.

While the method and system of the present invention are described herein as applied to visible light, providing particular benefits in the visible wavelength range of about 400nm-650nm, the method and system can also be applied to light having other wavelengths, for example to light in the near infra red (NIR) range of about 650nm-1000nm. Also, the method and system apply equally well to a system in which the light transmitted by the laser is in one wavelength range, for example, in the visible range, and the light emitted by the fluorescent proteins is in another wavelength range, for example in the NIR range. The method and system also apply where both the light transmitted by the laser and the light emitted by the fluorescent proteins are in the NIR range. Also, light beyond the wavelength range of 400nm-1000nm can be used.

This invention provides modified expressions of the diffusion approximation, combined with appropriate normalization schemes for enabling three-dimensional tomographic imaging of fluorescent proteins in-vivo in a visible wavelength range of about 400nm-650nm. The modified expressions of the diffusion approximation do not require the use of the more complex transport equation. Therefore the modified solutions obtain computational efficiency.

The method and system for optical tomography using fluorescent proteins includes modified expressions of the diffusion approximation combined with appropriate data collection concepts and instrumentation for three-dimensional imaging of fluorescent proteins in diffuse media, for example, in living tissue. The use of modified expressions of the diffusion approximation provides practical and computationally efficient reconstruction schemes. The method and system are significantly different than those used for conventional imaging in the near infrared (NIR).

The method and system for optical tomography provide multiple projection imaging using visible light. In some embodiments non-contact tissue illumination and/or non-contact light reception is used, wherein light sources and/or light sensors are spaced apart from the object being scanned.

The method and system of the present invention using visible light provides higher spatial resolution than conventional tomographic approaches using near-infrared (NIR) light and yield quantification and sensitivity superior to conventional planar imaging with fluorescent proteins. This new modality can be applied to visualize a variety of biological and molecular processes by using a variety of different fluorescent proteins. For example, in various embodiments, fluorescent proteins can be used to monitor tumor growth, metastasis formation, gene expression, and therapeutic effects. In addition, the method and system can be used to provide non-invasive, whole-body molecular imaging to non-invasively yield information associated with activity at sub-cellular levels.

In one particular embodiment, the method and system of the present invention include the optical scanner light source used in place of the conventional optical scanning switch, providing other advantages. The other advantages include, but are not limited to, lower energy losses through the optical scanner light source as compared to energy loss though the conventional optical scanning switch, uniform response over a number of apparent light sources, and improved reliability and robustness. Also, the scanning area as well as the number and spatial configurations of the apparent light sources are software controlled and can be varied in accordance with characteristics of the object being scanned. Furthermore, higher power illumination and a wider wavelength range (e.g., from 400 to 1000 nanometers) can be achieved.

The method and system of the present invention allow trans-illumination through living tissue, reduction of auto-fluorescence effects, increased resolution resulting from higher absorption of visible light and corresponding lower spatial spread, and three-dimensional imaging and quantification of fluorescent proteins not previously available.

The emitted fluorescent light provided by embodiments of the present invention can be continuous wave (CW) light, time-resolved (TR) light, or both CW and TR light. In addition, the method and system of the present invention can give information on the dynamics of the

system as function of time, and the resulting image can be co-registered with an image obtained by another imaging method such as magnetic resonance imaging (MRI), computed tomography imaging (CAT), ultrasound or bioluminescence imaging.

In operation, the method and system of the present invention can provide insight into specific molecular and biological abnormalities that form the basis of many diseases, e.g., cancer, tumor growth, and metastasis formation. The method and system can also be used to image angiogenesis since the high absorption of hemoglobin contrasts the vessels against the fluorescent background of the tumor cells. Furthermore, the method and system can be used to assess efficacy of novel targeted therapies at a molecular level. This, in turn, can have an impact on drug development, drug testing, and choosing appropriate therapies and therapy changes in a given patient. Still further, the method and system enable study of the genesis of diseases in the intact microenvironment of living systems. And, still further, the method and system are useful for testing novel gene delivery strategies. The imaging method and system allow acquisition of three-dimensional information much faster than is currently possible with time consuming and labor intensive conventional basic science techniques.

The method and system of the present invention have broad applications in a wide variety of biologic, immunologic, and gene therapies designed to promote the control and eradication of a variety of diseases including cancer, neurodegenerative, inflammatory, infectious, and other diseases. Furthermore, the method and system have broad applications for seamless disease detection and treatment in combined settings.

BRIEF DESCRIPTION OF THE DRAWINGS

The foregoing features of the invention, as well as the invention itself may be more fully understood from the following detailed description of the drawings, in which:

Figure 1A is a block diagram of an optical tomography having a laser source, a light delivery optical fiber, an optical scanning switch, a cooled CCD detector, and an imaging plate;

Figure 1B is a top view of the imaging plate of Figure 1A depicting an array of thirty-three apparent light sources;

Figure 2A is a photograph of an optical scanner used in an alternate embodiment in place of the optical switch of Figure 1;

Figure 2B is a block diagram of optical scanner of Figure 2A, showing adjustable input optics with a fiber coupler, galvo-controlled mirrors, and a telecentric lens used for the production of a flat light field and a plurality of apparent light sources at a constant working distance (WD);

Figures 3A and 3B shows a series of thirty-three images, corresponding to the thirty-three apparent light sources of Figure 1 taken with the optical scanner of Figure 2B, showing intrinsic (i.e., transmitted light) and fluorescence fields used for the calculation of a composite Born field;

Figure 4A shows a series of thirty-three images of the apparent light sources taken with the optical scanner of Figure 2B;

Figure 4B shows a series of thirty-three images of the light sources obtained through a homogeneous slab (i.e., a phantom) taken with the optical scanner of Figure 2B;

Figure 5 is a flow chart showing an exemplary process used to provide a tomographic image in accordance with the present invention;

Figure 6 is a graph showing experimental measurements of fluorochrome concentrations and actual fluorochrome concentrations in test objects;

Figures 7A-7C show fluorochromes in test objects closely spaced in a plane and imaging resolutions thereof;

Figure 8 shows fluorochromes in test objects closely spaced in the plane of Figure 7D and closely spaced perpendicular to the plane of Figure 7D and imaging resolutions thereof;

Figures 9 and 9B show a white light image of a dead mouse placed inside an imaging chamber after placement of glass vials with green fluorescent protein (GFP) expressing cells into the esophagus;

Figures 10A-10C show a white light image of a live mouse placed inside the imaging chamber after subcutaneous injection of GFP expressing cells;

Figure 11A is a block diagram of a system for optical tomography having a time resolved system employing an ultra-fast laser and an intensified gated CCD and having a planar imaging geometry;

Figure 11B is a block diagram showing an imaging chamber used in the system of Figures 11A;

Figure 12 is a block diagram of an alternate system for optical tomography having the planar imaging geometry of the embodiment of Figure 11 and a rotating stage; and

Figure 13 is a block diagram of another alternate system for optical tomography having a cylindrical imaging geometry;

Figure 14 is a block diagram yet another alternate system for optical tomography having a cylindrical imaging geometry;

Figure 15 is a block diagram yet another alternate system for optical tomography having a planar imaging geometry; and

Figures 16A and 16B show yet another alternative embodiment for optical tomography in which transillumination measurements are combined to yield transillumination images.

DETAILED DESCRIPTION OF THE INVENTION

Before describing the method and system for optical tomography using fluorescent proteins, some introductory concepts and terminology are explained. As used herein, a "phantom" refers to a test object being scanned. A phantom is typically a manufactured article having diffuse light propagation characteristics similar to living tissue, for example, a piece of plastic. For another example, a phantom can be a vial having cells expressing the fluorescent proteins therein. As used herein, the term "apparent light sources" is used to describe projections of a single light source to a plurality of physical positions or angles.

Referring now to Figures 1A and 1B, a block diagram in Figure 1A shows exemplary apparatus adapted to generate tomographic images associated with fluorescent proteins. The apparatus includes a laser, an optical fiber, and an optical switch, which in combination generate a plurality of apparent light sources upon an imaging plate and upon a subject, here shown to be a mouse placed in a chamber having a matching fluid. The laser light enters the subject and excites fluorescent proteins to generate fluorescent light. The apparatus also includes a CCD camera to receive the laser light and the fluorescent light and an image processor having a diffusion equation processor, the image processor adapted to receive and

process electrical signals from the CCD camera. A graphical display can be provided to display resulting image information.

An Argon (Ar^+) laser emitting approximately 200mW continuous wave (CW) power at approximately 488nm can be used for excitation of the fluorescent proteins. The laser light is delivered through a 100μm diameter multimode fiber to an input collimator (not shown). The single laser light is used to provide a plurality of apparent light sources at different physical positions by way of an optical switch. In one particular embodiment, the optical switch provides thirty-three apparent light sources, as indicated in the planar inset in Figure 1B. However, in other embodiments, more than thirty-three or fewer than thirty-three apparent light sources can be provided.

Though an optical switch is shown, in one particular embodiment, the optical switch can be replaced with an optical scanning head (or optical scanner), shown in greater detail in Figure 2. The optical switch or the optical scanner provides transmitted light at a variety of angles (i.e., a plurality of apparent light sources), thereby providing a variety of images that can be combined in a tomographic process. It will be understood that the optical switch includes a plurality of selectable optical fiber paths (not shown), adapted to direct light to a corresponding plurality of selectable fixed physical locations, providing apparent light sources that are selectably fixed in position and number. It will be further understood in conjunction with Figure 2B that the optical scanner can be software controlled to provide apparent light sources that are selectably variable in position and number

Living tissue, here shown to be a mouse, is placed on a plate (Figure 1A), in contact with an optical matching fluid. The matching fluid is further described below. In operation, light from each of the apparent light sources (e.g., see Figure 1A) and also light generated by fluorescent proteins within the subject are received by a CCD camera and thereafter tomographically processed as described in conjunction with Figure 5. In one particular embodiment, the CCD camera is cooled to reduce dark noise.

Figure 1B

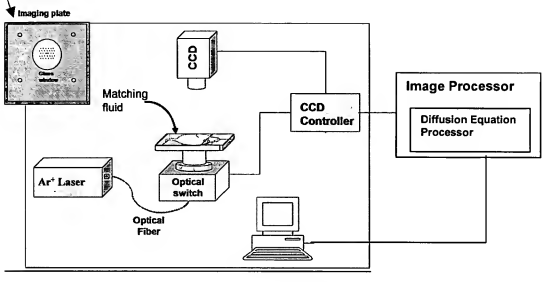

Figure 1A

Referring now to Figures 2A and 2B, an exemplary optical scanner, used in place of the optical switch of Figure 1, can employ two galvanometer controlled mirrors and a scan lens (telecentric lens) for scanning and focusing the laser beam onto an input window of the chamber (Figure 1), to provide a plurality of apparent light sources, each at a different physical position. In one particular embodiment, the beam diameter at the focus plane is approximately 300μm. The light delivery can be performed with a single fiber from a single laser source.

The optical scanner provides a non-contact configuration having little optical loss compared to optical losses of a conventional optical switch. The prior art optical switch mentioned in conjunction with Figure 1 has a variety of disadvantages, including, but not limited to, coupling losses of the optical switch, and losses within each source fiber, each of which can be easily damaged. Thus, the present optical scanner provides a more reliable and robust light source system. Furthermore, with the present optical scanner, a scanning area, a light beam shape, as well as a number of apparent light sources and apparent light source positions can be varied (software controlled). Also, a higher light power delivery and a wider

light wavelength range (visible light to near infrared (NIR) light)) can be achieved. A schematic of an exemplary array of apparent light sources shown in the inset of Figure 1 can be provided, for example, with the optical scanner of Figure 2.

A central apparent light source at a center of the field of view (point (0, 0)) can be used to co-register a white light image with the tomographic images taken with different light filters (further described below) and also with the final tomographic reconstruction.

Figure 2A

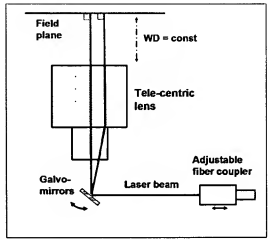

Figure 2B

The light detection is made with a light sensor, which can include a highly sensitive, cooled CCD camera having reduced dark noise. For example, the CCD camera can be provided as a Roper Scientific, Princeton Instruments CCD camera with a cryogenic cooling unit. During acquisition, the scanning head (optical scanner, Figure 2) is controlled and triggered by the CCD camera's controller (Figure 1) so that each obtained image corresponds to a new position of the scanning mirrors (i.e., a different apparent source), thus achieving the proper synchronization of excitation and detection. Each acquisition is composed of N images, one for each apparent light source position. Therefore, assuming a 512x512 pixel CCD camera, a maximum number of data for each set of measurements is Nx512x512, which enables high accuracy measurements. However, the number of detectors (i.e., pixels) used for the reconstruction can be smaller than the full group of 512x512 pixels depending on the field

of view defined by the array of apparent sources. Also, the number of pixels used can be reduced to reduce computational time required for image processing

A subject to be scanned can be placed horizontally on an imaging plate (Figure 1) and compressed with a covering glass. The chamber is then filled with an Intralipid and India ink solution, which provides a match to optical properties and minimizes the index of refraction and diffuse-wave mismatches in the chamber. Breathing of the subject being scanned during in vivo studies can continue normally through the entire process since the glass window covers the subject body up to the chest, leaving the head and nose well above the liquid surface.

In one particular embodiment, the solution consists of 1% intralipid and 2.1% ink, which corresponds to μ_a=1.25cm^{-1} and μ_s'=16.7cm^{-1} for absorption and reduced scattering coefficient respectively.

The light propagation inside the diffuse media (i.e., the subject) was modeled using the modified Diffusion Approximation for high absorbing media derived from the Radiative Transport Equation. Both the intrinsic field generated by the laser excitation light and the fluorescence field which is generated inside the medium due to a fluorochrome at a position $\vec{r}$ are calculated independently and then used to calculate the normalized Born field, which is used in a reconstruction algorithm. The Born field $U_c(\vec{r}_s,\vec{r}_d)$ at the light detectors' position $\vec{r}_d$ due to a source at position $\vec{r}_s$ in a medium with a modified diffusion coefficient and propagation wave numbers that account for high absorption is given by:

$$U_c(\vec{r}_s,\vec{r}_d) = S_o \frac{U_{fl}(\vec{r}_s,\vec{r}_d) - \Theta_f U_{inc}(\vec{r}_s,\vec{r}_d)}{U_{inc}(\vec{r}_s,\vec{r}_d)} = \frac{1}{U_o(\vec{r}_s-\vec{r},k^{\lambda_1})} \int d^3r \cdot U_o(\vec{r}_s-\vec{r},k^{\lambda_1}) n(\vec{r}) \frac{\upsilon}{D^{\lambda 2}} G(\vec{r}_d-\vec{r},k^{\lambda_2}) \quad (1)$$

where $U_{fl}(\vec{r}_s,\vec{r}_d)$, $U_{inc}(\vec{r}_s,\vec{r}_d)$ are measurements at the emission and excitation wavelengths respectively, $U_{bl}(\vec{r}_s,\vec{r}_d) = \Theta_f U_{inc}(\vec{r}_s,\vec{r}_d)$ is the bleed through signal, Θ_f is a band-pass filter attenuation factor, S_o is a gain term that accounts for instrument gain differences at the excitation (λ_1) and emission (λ_2) wavelengths, $n(\vec{r})$ is the product of the fluorochrome

absorption coefficient and fluorescence quantum yield, k^{λ_1} k^{λ_2} are the modified photon wave propagation wavenumbers at λ_1 and λ_2 respectively which account for high absorption, υ is the speed of light into the medium, D^{λ_2} is the modified diffusion coefficient in the presence of high absorption at λ_2, $U_o(\vec{r}_s - \vec{r}, k^{\lambda_1})$ is a term that describes the established photon field at position $\vec{r}$ into the medium at λ_1, and $G(\vec{r}_d - \vec{r}, k^{\lambda_2})$ is the Green's function solution to the diffusion equation that describes the propagation of the emission photon wave from a fluorochrome at position $\vec{r}$ to the detector given by:

$$G(\vec{r}_d - \vec{r}, k^{\lambda_2}) = \frac{\exp(ik^{\lambda_2}(\vec{r}_d - \vec{r}))}{(\vec{r}_d - \vec{r})} \qquad (2)$$

An advantage of using the normalized expression is that all the position-dependent contributions are eliminated, and more importantly, this field can be calculated even with the presence of the fluorochrome. This means that no background measurements before the administration of the agent are necessary which is important for in vivo studies.

A useful way to represent the absorption dependence of the diffusive light propagation is by writing the diffusion coefficient as:

$$D = \frac{1}{3(\mu_s' + a\mu_a)} \qquad (3)$$

where a will generally depend on the absorption, scattering, and anisotropy of the medium. In terms of the scattering coefficient μ_s we recall that the reduced scattering coefficient is written as $\mu_s' = (1-g)\mu_s$. A simple expression for the diffusion coefficient D that accounts for high absorption may be found through derivation from the Radiative Transport Equation, obtaining:

$$D = \frac{1}{3(\mu_s' + \mu_a)}\left(1 - \frac{4}{5}\frac{\mu_a}{\mu_s'(1+g) + \mu_a}\right)^{-1} \qquad (4)$$

Note that here we have chosen to express D in terms of the reduced scattering coefficient μ_s', which is the relevant quantity in scattering experiments in anisotropic media. One main difference between Eq. (4) and most commonly used expressions (namely with a=0 or a=1) is that in this case the value of the anisotropy factor, g, must be known *a priori*. From Eq. (4) we

see that the diffusion coefficient depends nonlinearly on the scattering and the absorption properties of the medium. The expression for a is found from Eq. (4) and Eq. (3) as:

$$\alpha = 1 - \frac{4}{5}\frac{\mu_s' + \mu_a}{\mu_s'(1+g) + \mu_a} \tag{5}$$

Typical values of α range from 0.2 to 0.6 being in the order of 0.5 – 0.55 in the case of tissue in the visible, assuming an anisotropy factor of g~0.8, which is typical for tissue. The dependence of α with g is a very slight one, where changes in the value of g within realistic biological values (g between 0.5 and 0.9) give small changes in the value of α. It will be understood that if the classical descriptions of the diffusion coefficient are used (namely with α=0 or α=1), the diffusion approximation yields inaccurate results. This is the reason why it has been long thought that the diffusion approximation fails in the presence of high absorption. However, when the modified absorption coefficient is used, the diffusion approximation still holds. To that end, a modified wavenumber must be defined, namely:

$$k^{\lambda} = \sqrt{-\frac{\mu_a^{\lambda}}{D_a^{\lambda}} + \frac{i\omega}{vD_a^{\lambda}}} \tag{6}$$

where ω is the modulation frequency (in the CW case, ω=0). Based on a modified expression for the diffusion coefficient combined with appropriate changes in the wave propagation wavenumber, Green's function solutions to the diffusion equation can be derived that are appropriate for imaging in the visible range of light.

The different optical properties are calculated by fitting the diffused patterns obtained after transmission through a homogeneously scattering slab (i.e., a phantom). The width of the diffused patterns in this case is smaller, thus they are more confined around the central, straight trajectory. This is an effect of the higher absorption and higher scattering of tissue in the visible range of light. This happens because the photons that are multiply scattered have a higher probability of absorption because of their longer path length than the ones that propagate in more straight trajectories. The effect is similar to the effect of early temporal gating of the received light, where only the early arriving and least scattered photons are selectively detected making the distribution of light spatially narrower and the resolution achieved significantly better.

Referring now to Figures 3A and 3B, two types of measurements are acquired: fluorescence measurements using band-pass interference filters centered on the fluorescence emission, and intrinsic light measurements obtained by using band-pass interference filter centered on the laser emission. The exposure times can be varied so that dynamic range is maximized. These measurements are used to generate the field $U_c(\vec{r}_s, \vec{r}_d)$. This approach can be applied in all embodiments of the method both in trans-illumination and front illumination schemes in both planar and cylindrical geometries. One advantage of using this normalized field is that it reduces all positional inhomogeneities and inaccuracies and it can be calculated even with the presence of a fluorochrome eliminating the need for background measurements.

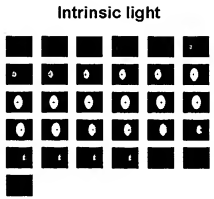

Figure 3A

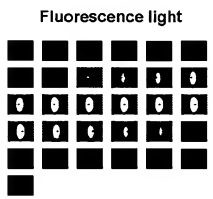

Figure 3B

Referring now to Figures 4A and 4B, before the acquisition of the FMT images of Figures 3A and 3B, a white light image is acquired as well as a series of images of the intrinsic light through the homogeneous slab so that the location of the sources can be calculated for each individual measurement. This procedure improves the co-registration of white light and tomographic images, reducing any errors.

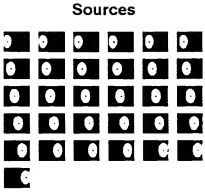

Figure 4A

Figure 4B

Referring now to Figure 5, in order to reconstruct the three-dimensional fluorochrome distributions using the composite field measurements, the volume of interest can be segmented into axial (horizontal) layers (e.g., 21) containing a number (e.g., 651) of voxels each. The voxel size depends on the dimension of the field of view and the number of segmentations. A forward model (i.e., a model of light distribution in the medium) is constructed using the algorithm described above and inverted (i.e., solved) using algebraic reconstruction techniques with positive restriction. Typical inversion times are on the order of 10 min on a 2 GHz Intel Pentium 4 processor. Reconstructed images display the fluorochrome concentration in 3D. An exemplary FMT process in accordance with the present invention can be seen in the flow chart of Figure 5.

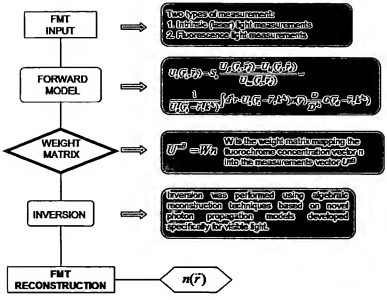

Figure 5

Referring now to Figure 6, a graph includes a curve of reconstructed fluorochrome concentration values and a curve of actual fluorochrome concentration values associated with test objects. The ability of the system to quantify fluorochrome concentrations was assessed by a titration experiment in which thin glass tubes with different (150nM, 300nM, 600nM and 1200nM) concentrations of fluorochrome (Fluorescein Isothiocyanate – FITC) were imaged. They were placed at the center of the field of view and at a depth of 6mm from the input glass window. The acquisition was performed as described in above with a laser power of 100mW.

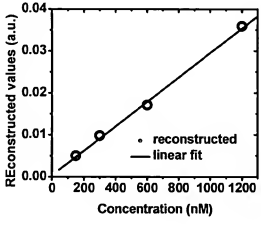

Figure 6

Referring now to Figures 7A-7C, spatial resolution is evaluated by imaging phantoms constructed of two glass tubes containing the same concentration of the fluorochrome placed parallel at the center of the field of view, at the same depth and at varying separations (0.5mm, 0.7mm, 1mm and 1.5mm). These distances represent the clear gap between the two tubes and not the actual separation of the fluorochrome solution, which is larger. The laser power was 100mW while a linear source array with 31 apparent light sources at a distance of approximately 500μm between them was used to increase performance. Reconstructed images are shown in Figure 7C, where axial cross sections of the tubes at the center of the field of view are depicted.

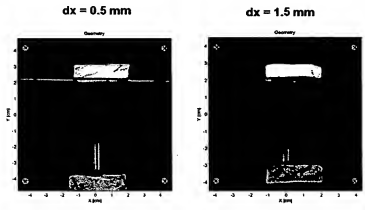

Figure 7A Figure 7B

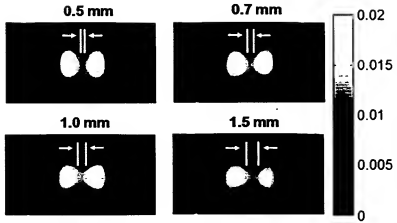

Figure 7C

Referring now to Figure 8, resolving power of the device in the z (trans-illumination) direction is shown by imaging a resolution phantom in which two glass tubes with different concentrations (600nM and 1200nM) are placed at a different depth. The horizontal clear gap between the two tubes was 1mm whereas the vertical one was 0.5mm, with the higher concentration tube being deeper. Figure 8 shows the reconstructed image where an axial cross section is depicted as above, showing two clear foci at the positions of the tubes. The reconstructed value of the deeper tube was 4.6 times higher.

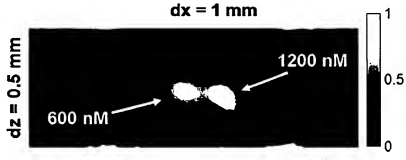

Figure 8

The corresponding resolution measured with similar experimental and reconstruction configurations with an NIR FMT system was 0.7mm. These results show that the spatial resolution achieved using light having visible wavelengths is higher than that obtained using NIR light. The higher resolution can be attributed to the higher absorption of visible photons compared to NIR photons, which eliminates the contribution of the highly diffused photons to the recorded diffused pattern. The result is that only the photons traveling around the central path will be able to reach the detector.

The results described above are representative of but one experimental embodiment. It can be expected, that in other embodiments, still greater resolution can be achieved.

Referring now to Figures 9A and 9B, an example of imaging capability of the method and system of the present invention is shown. Two different numbers of green fluorescent protein (GFP) expressing tumor cells were used: 10^5 and 10^6. They were placed inside thin glass tubes

and inserted in the esophagus of animals after they had been sacrificed. The animals were placed inside the imaging chamber, which was then filled with the matching fluid described above. Imaging was performed using the 33 apparent light source array trans-illuminating the area around the chest of the animal. The goal was to investigate the ability of the system to quantify GFP fluorescence signals originating from deep tissue.

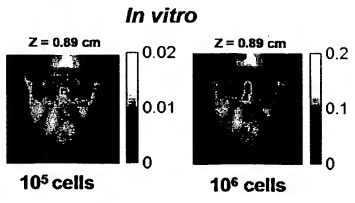

Figure 9A Figure 9B

Referring now to Figures 10A-10C, another example of imaging capability of the method and system of the present invention is shown. The method and system can be used for whole body imaging of gene expression in vivo. Two sagittal cross sections at different depths defined by the z value of subcutaneously injected GFP expressing cells are presented.

Results shown are examples only, and it can be expected that the method and system can image an even smaller number of cells, and that sensitivity corresponds to lower concentrations than those shown.

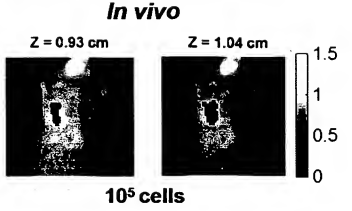

Figure 10A Figure 10B Figure 10C

Referring now to Figure 11A, in one particular embodiment, the system for optical tomography of the present invention includes a planar imaging geometry. Figure 11B shows a close-up of an exemplary imaging chamber having a planar configuration. The capability of operation in a wide wavelength range and of high power delivery enables the system to operate with ultra-fast lasers for time resolved and fluorescence lifetime imaging, potentially improving the resolution and the contrast of imaging. The same setup could be implemented in a variety of imaging modalities because of its wide spectral range of operation and capabilities of light delivery, ranging from CW systems in the NIR range of light to time resolved systems with high power ultra-fast pulsed lasers for early time detection and fluorescence lifetime imaging.

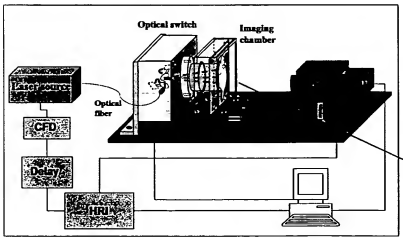

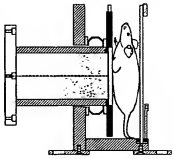

Figure 11A Figure 11B

Referring now to Figure 12, an alternate embodiment of the system for optical tomography includes a planar geometry similar to the geometry of Figure 11. The planar geometry (e.g., Figure 11) is combined with a rotation stage. The rotating stage provides a large number of apparent light source angles relative to the object being scanned. Using visible light for tomographic imaging results in the fewer obtained projections, which impair the imaging quality. This can be overcome by using the alternate geometry of Figure 12, which offers a large number of detection angles. With this embodiment, high quality 3D imaging can be achieved.

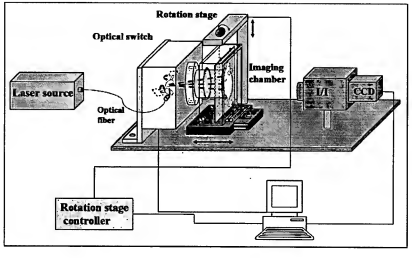

Figure 12

Referring now to Figure 13, another alternate embodiment of the system for optical tomography provides a cylindrical geometry. The same high quality 3D imaging provided by the embodiment of Figure 12 can be achieved with the cylindrical geometry. An advantage of the cylindrical geometry is that both the rotation as well as the imaging algorithm is simpler and faster, without imposing drawbacks on the image quality.

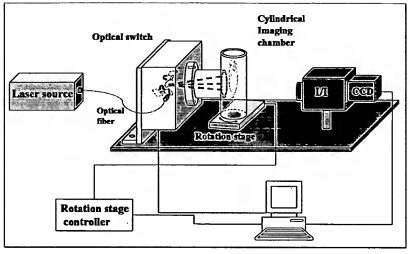

Figure 13

Referring now to Figure 14, yet another alternate embodiment of the system for optical tomography provides a cylindrical geometry with a single fiber, which can be scanned in the z direction (along the length of the cylinder comprising the imaging chamber). The same high quality 3D imaging provided by the embodiment of Figure 13 can be achieved with this simpler configuration. An advantage of the cylindrical geometry is that both the rotation as well as the imaging algorithm is simpler and faster, without imposing drawbacks on the image quality.

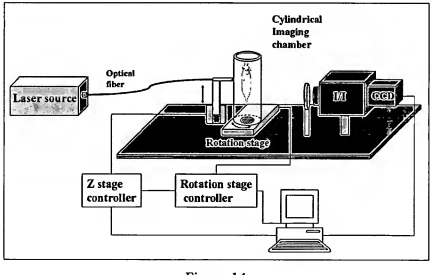

Figure 14

Referring now to Figure 15, another embodiment of the imaging system incorporates a planar geometry with an array of fibers (a) scanned in x and y directions and illuminating all together at the same time. Advantages of such an embodiment include, but are not limited to, faster acquisition when low signals impose long exposure times. Crosstalk between the fibers can be minimized by appropriate selection of distances between the individual fibers so that the paths of the propagating photons do not overlap. In applications where exposure times can be short, the fibers can be alternatively illuminating one at a time to eliminate noise from crosstalk. In this embodiment the optical scanner described in conjunction with FIGS. a fiber switch replaces 2A and 2B. In an alternate embodiment, a single fiber can be scanned in the x and y directions, which can be used in different illumination schemes; (b) a collimated or (c) a focused beam employing miniaturized optics or appropriate engineering of the fiber tip. In an alternate embodiment (d) the beam could be expanded to produce a larger illumination pattern to cover the whole scanned area and increase throuput capacity. Similar planar imaging can be realized by using (e) a fine grid of fibers, which will produce a homogeneous illumination pattern. The above illumination schemes can be scanned in the x and y direction to cover the whole area under investigation and can be employed in both trans-illumination and front illumination schemes.

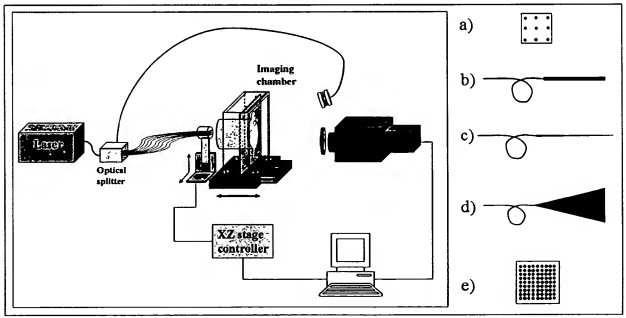

Figure 15

In an alternate embodiment the illumination and detection can be done by employing a taper system for delivery and/or collection of light instead of the array of fibers, which could produce either a single or multiple point illumination (as described above) or an expanded illumination pattern. This alternate system could be used both for trans-illumination tomography and reflection tomography.

Referring now to Figures 16A and 16B, another embodiment of the imaging system provides transillumination views of the object in the absence of reconstruction. Raw transillumination measurements can be employed in cases where fast visualization is of importance, at the expense of reduced depth resolution. These views offer significant advantages over front illumination methods since they minimize recorded autofluorescence from the surface of the object being scanned (which occurs in front illuminated views) while retaining detection sensitivity close to that of tomography. Images can be formed by plotting the field Uc (left part of Eq.1) either for a single $\vec{r}_s$ position or as $U_c' = \sum_i^{N_i} U_c(\vec{r}_{s_i}, \vec{r}_d)$.

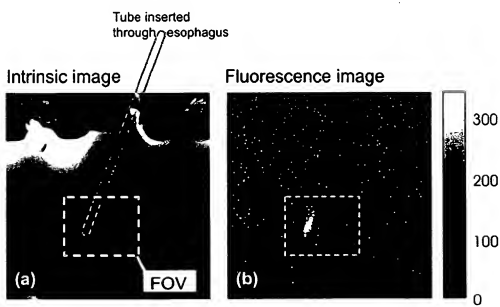

Figure 16A

Figure 16B

The method and system of the present invention can be in combination with newly developed fluorescent proteins, namely DsRed and HcRed, because of their emission characteristics in the red region of the spectrum. This combination can increase the signal detection efficiency because of the larger penetration depth compared with visible light and still maintain higher resolution than NIR systems.

The method and system of the present invention can be used for studying tumor growth and monitoring of metastasis formation when used with tumor cells that express fluorescent proteins (like GFP).

The method and system of the present invention can be used with GFP expressing tumor cells and YFP expressing viral cells for the study of gene delivery and gene therapy for specific patient targeted treatment. The signals from the two or more fluorochromes can be spectrally decomposed using linear unmixing algorithms for independent imaging of each fluorescence signal in order to target different biological process simultaneously.

The method and system of the present invention can be implemented such that they take advantage of novel imaging modalities using newly developed algorithms for imaging arbitrary geometries without the need of the optical properties of matching fluids. The algorithms for modeling of light propagation and solving inverse problems can be applied to all of the above system embodiments and geometries.

All references cited herein are hereby incorporated herein by reference in their entirety.

Having described preferred embodiments of the invention, it will now become apparent to one of ordinary skill in the art that other embodiments incorporating their concepts may be used. It is felt therefore that these embodiments should not be limited to disclosed embodiments, but rather should be limited only by the spirit and scope of the appended claims.

Fluorescent Protein Tomography

Invention consists of NEW USE of imaging methods and devices to apply to a novel imaging method "visible light fluorescence tomography"; the invention includes a derivative method to reconstruct/analyze images

Closest existing technologies:
NIR (near infra-red) tomography

whole body optical imaging: surface ≤ 1mm tomography (photographic or CCD camera picture of fluorescent surface tissue) or whole-body imaging transilluminated microscopy.

Company in technology field
AntiCancer Inc. fluorescence tomography imaging in *in vivo* surface tissue ≤ 1 mm or with a trans-illuminator/light box

New Use in tomography:
new method to generate data, no visible light fluorescence tomography published

applying visible (exciting and emitting) light, 450-650nm
applying lasers as visible light source
non-contact tissue illumination, light beam instead of fiber guided light to target.
multiple projection imaging

new method (new physical model) **to analyze/reconstruct the image**: new model to enable imaging lies between x-ray and NIR tomography

Advantage of new system over NIR tomography:
Maximizing projection, transillumination becomes feasible
improved three-dimensional imaging
Higher spatial resolution
Computationally more simplistic.

Use in transillumination:
Method to obtain planar field transillumination measurements, consists of back-illuminating with planar filed or time-shared individual spots that are then added together at post-processing. Transilluminaiton is not new, however using transillumination views in FP tomography (or FP in the visible more generally) will have a very interesting application and would be much more important than transillumination applied in the NIR, because of the more straight photon propagation.

Problems addressed by the invention:

The new methods and systems can provide insight into specific molecular and biological abnormalities that form the basis of many diseases, e.g. cancer, tumor growth and metastasis formation, as well as imaging angiogenesis and consequently assess the efficacy of novel targeted therapies at a molecular level. This, in turn, is expected to have an impact in drug development, drug testing, and choosing appropriate therapies and therapy changes in a given patient as well as testing novel gene delivery strategies. Furthermore, the new fluorescent protein imaging/quantitation methods and systems potentially enable one to study the genesis of diseases in the intact microenvironment of living systems. Finally, the imaging methods allow one to gain three-dimensional information that is much faster to obtain than is currently possible with time consuming and labor intensive conventional, basic science techniques.

Existing solutions to the problems:

There are no methods currently for whole body fluorescence protein imaging.

Existing solutions for imaging fluorescing engineered proteins include epi-fluorescence, confocal (microscopy) or reflectance imaging that are NOT quantitative and reach depths of a few hundred microns (microscopy) to a few millimeters (reflectance imaging). Microscopy has also very limited fields of view (~1x1mm^2) to allow for whole animal imaging. Reflectance imaging has been shown useful in detecting and following tumors in vivo, particularly those implanted near the surface or in surgically exposed organs. However, reflectance imaging has significant inherent limitations, since the recorded images are a superposition of fluorescence signals from multiple depths, each correspondingly blurred. Thus, it does not retrieve depth information nor allow absolute quantification of fluorescence activity.

Furthermore, existing methods for modeling photon propagation and perform fluorescence reconstructions through whole animal bodies are based on the assumption that light is transmitted through highly scattering but low absorbing media (which is mathematically essential for the derivation of the diffusion approximation to the transport equation). However, this approach can not be applied in the visible where the high absorption of tissue alters the propagation of light significantly. Other approaches that use the solution of the transport equation and can be more accurate are computationally very expensive and become impractical for dealing large data sets and they have never been applied to imaging in the visible so far and to the best of our knowledge. In addition light delivery technologies that may be appropriate for whole body animal imaging in the NIR may become inadequate for imaging in the visible and should be explicitly considered for appropriate instrument design.

Key aspects to the invention that make it unique and provide advantage over existing solutions:

The invention is based on the discovery that modified solutions of the diffusion equation, combined with appropriate data collection concepts and instrumentation can be used for three-dimensional imaging of fluorescent proteins in small animals.

The reconstruction mainframe suggested herein is significantly different than approaches previously proposed for imaging in the near-infrared. The technology development teaches that multiple projection imaging is essential for imaging in the visible and that non-contact tissue illumination is preferred for efficient instrumentation design.

Moreover the use of modified solutions of the diffusion equation is a key element for practical and computationally efficient reconstruction schemes. These new developments lead to unprecedented performance in terms of spatial resolution compared to tomographic approaches previously developed for the near-infrared and yield superior quantification and sensitivity compared to planar imaging approaches available so far for imaging fluorescent proteins.

Overall, the new methods and systems provide various advantages over existing modalities. These include lower coupling losses through the optical scanning switch compared to previously reported designs, uniform response over the whole number of sources, as well as the improved reliability, and robustness of the system. Second, the scanning area as well as the number and the spatial configuration of the sources are software controlled and can be varied according to the needs of the specific case. Third higher power delivery and a wider wavelength range (depending on the optical components that are used can be from the Visible to the NIR) can be achieved. This makes feasible imaging of a wide range of different fluorescing proteins such as GFP, YFP, DsRed and HcRed, individually or in a combined use of two or more proteins for visualization of biological processes such as gene delivery and therapy. Using proteins that emit in the red (DsRed and HcRed) instead of green (GFP) or yellow (YFP) can increase the imaging depth and improve imaging capabilities.

The combined effect of the improved design is that trans-illumination through the animal becomes feasible leading to reduction of auto-fluorescence effects common to planar illumination methods, increased resolution and three-dimensional imaging and quantification of fluorescent proteins not previously available in any existing method.

Potential products, processes, services or research tools based on the invention:

The new imaging systems and methods will have broad applications in a wide variety of novel biologic, immunologic and gene therapies designed to promote the control and eradication of numerous different diseases including cancer, neurodegenerative, inflammatory, infectious, and other diseases. Furthermore, the described detection systems and methods will have broad applications for seamless disease detection and treatment in combined settings, making it a very powerful and versatile tool for biological research. Potential products include small animal imaging systems for both three-dimensional tomographic imaging and visualization of fluorescent proteins and simple trans-illumination imaging as a high throuput testing device.

Patient or consumer base for such products, processes, services or research tools:

Pharmaceutical companies and research laboratories involved in many different aspects of biomedical, biological and genomics research. Fluorescent protein based research is very common and therefore advanced visualization tools may find significant applications.

TOMOGRAPHY OF FLUORESCENT PROTEINS

TECHNICAL FIELD

This invention relates to extracting quantitative, three-dimensional molecular and biological information from living mammals and patients using fluorescent proteins in transgenic cells and new optical tomographic imaging methods.

BACKGROUND

Fluorescence proteins (FP's) have become essential reporter molecules for different biomedical applications. Most frequently, engineered FP's are detected by epi-fluorescence, confocal (microscopy) or reflectance (whole animal) imaging. The latter has been shown to be useful in detecting and following tumors in vivo, particularly those implanted near the surface or in surgically exposed organs. However, reflectance imaging has inherent limitations, since the recorded images are a superposition of fluorescence signals from multiple depths, each correspondingly blurred. Thus, it does not retrieve depth information nor allow absolute quantification of fluorescence activity. This is mostly due to strong non-linear light attenuation and propagation in biological tissues and limits the applicability of the technique to semi-quantitative imaging of objects at depths of only a few millimeters.

Imaging optical signatures deeper in tissues requires the application of advanced excitation-detection schemes and the use of tomographic principles for combining data acquired at different projections. Advances in imaging with diffracting sources have resulted in several studies investigating tissue using intrinsically or extrinsically administered optical contrast. In particular, Diffuse Optical Tomography (DOT) is a technique that can resolve absorption and scattering in diffuse media and has been applied toward cerebral hemodynamic imaging and imaging of breast cancer patients.

Furthermore, compounds that fluoresce after light excitation have become valuable markers to sense and image a wide variety of biological processes. It has been shown that light with wavelengths in the near-infrared range can propagate through tissue for distances on the order of multiple centimeters, because of low tissue absorption in the so-called "near-infrared window". This finding has encouraged the development of fluorescence techniques to visualize specific biochemical events inside living subjects.

Related reconstruction methods for fluorescence signals have also been developed, and their imaging capacity has been demonstrated with simulated data and phantom measurements. The development of appropriate imaging systems has enabled the application of Fluorescence Molecular Tomography (FMT), a technique that resolves molecular signatures in deep tissues using fluorescent probes or markers. The performance of FMT *in vivo* in three-dimensional imaging of enzymatic activity in deep-seated tumors has been recently demonstrated in small animals.

A common element to all tomographic techniques developed for fluorescence reconstructions is that they assume propagation in diffuse media with high scattering and relatively low absorption values. This assumption is essential to derive the diffusion approximation to the transport equation as an effective tool for modeling photon propagation in tissues. However, tomographic imaging in the visible is complicated by

the high absorption of tissue, which results in significant attenuation. This reduces the applications to small animal imaging and renders the use of the theoretical models used in Diffuse Optical Tomography useless since the diffusion approximation is not valid anymore. More advanced solutions based on the transport equation have been proposed, which may solve the theoretical inadequacy of the diffusion equation for tomography in the visible. However solutions to the transport equations are generally computationally expensive and become impractical for tomographic systems employing large data sets. So far no transport-equation solutions are utilized mainly for imaging in media where highly scattering and void regions co-exist however no such solution has been demonstrated for the tomographic problem in the visible. In addition light delivery technologies that may be appropriate for imaging in the NIR may become inadequate for imaging in the visible and should be explicitly considered for appropriate instrument design.

Tomographic imaging of fluorescent proteins requires then 1) an appropriate and efficient tomographic mainframe for quantitative three-dimensional imaging, 2) appropriate data collection concepts are required to optimally interface to the type of data collected from highly absorbing environments and 3) an appropriate instrumentation design for small animal imaging that is also well suited to the different power requirements in the visible. This invention teaches on appropriate photon technologies and modified solutions of the diffusion approximation, combined with appropriate normalization schemes for enabling three-dimensional tomographic imaging of fluorescent proteins in-vivo in the wavelength range 400nm-650nm. The solutions employed are based on modified solutions of the diffusion equation and do not require the use of the more complex transport equation. Therefore they retain the computational and implementation simplicity common in tomographic schemes in the near-infrared region.

SUMMARY

While examples are given below having visible light (e.g., wavelengths of 400nm to 650nm), it should be appreciated that the invention applies equally well to light having other wavelength, for example to light in the near infra red wavelength range of about 650nm to 1000 nm. Furthermore, still other wavelength ranges can be used. Also, while examples are given below associated with animals and images of animals, the method and system apply equally well to any tissue, including human tissue, and to any diffuse medium.

The invention is based on the discovery that modified solutions of the diffusion equation, combined with appropriate data collection concepts and instrumentation can be used for three-dimensional imaging of fluorescent proteins in small animals. The reconstruction mainframe suggested herein is significantly different than approaches previously proposed for imaging in the near-infrared as will be explained in the following. The technology development teaches that multiple projection imaging is essential for imaging in the visible and that non-contact tissue illumination is preferred for efficient instrumentation design. Moreover the use of modified solutions of the diffusion equation is a key element for practical and computationally efficient reconstruction schemes. These new developments lead to unprecedented performance in terms of spatial

resolution compared to tomographic approaches previously developed for the near-infrared and yield superior quantification and sensitivity compared to planar imaging approaches available so far for imaging fluorescent proteins. This new modality can be applied to visualize various biological and molecular processes assuming different uses of fluorescent proteins. The prime targets of using fluorescent proteins could be monitoring tumor growth, metastasis formation, gene expression and therapeutic effects. In addition, the new methods provide non-invasive, whole-body molecular imaging to non-invasively yield information associated with activity at sub-cellular levels.

Overall, the new methods and systems provide various advantages over existing modalities. These include lower coupling losses through the optical scanning switch compared to previously reported designs, uniform response over the whole number of sources, as well as the improved reliability, and robustness of the system. Second, the scanning area as well as the number and the spatial configuration of the sources are software controlled and can be varied according to the needs of the specific case. Third higher power delivery and a wider wavelength range (depending on the optical components that are used can be from the Visible to the NIR) can be achieved. The combined effect of the improved design is that trans-illumination through the animal becomes feasible leading to reduction of auto-fluorescence effects common planar illumination methods, increased resolution owing to the higher absorption of visible photons and the subsequent lower spatial spread and three-dimensional imaging and quantification of fluorescent proteins not previously available in any existing method.

The emitted fluorescent light in these methods can be continuous wave (CW) light, time-resolved (TR) light, or both CW and TR light. In addition, the methods can be performed dynamically as function of time, and the image can be co-registered with an image obtained by another imaging modality such as magnetic resonance, computed tomography imaging, ultrasound or bioluminescence imaging.

The impact of the new imaging techniques is potentially enormous. First, the new methods and systems can provide insight into specific molecular and biological abnormalities that form the basis of many diseases, e.g. cancer, tumor growth and metastasis formation. Second, the new methods can be used to image angiogenesis since the high absorption of hemoglobin contrasts the vessels against the fluorescent background of the tumor cells. Third, the new methods can be used to assess efficacy of novel targeted therapies at a molecular level. This, in turn, is expected to have an impact in drug development, drug testing, and choosing appropriate therapies and therapy changes in a given patient. Fourth, the new fluorescent protein imaging/quantitation methods and systems potentially enable one to study the genesis of diseases in the intact microenvironment of living systems. Fifth, the new methods of fluorescence-mediated optical tomographic imaging are useful for testing novel gene delivery strategies. Sixth, the imaging methods allow one to gain three-dimensional information that is much faster to obtain than is currently possible with time consuming and labor intensive conventional, basic science techniques.

The new imaging systems and methods will have broad applications in a wide variety of novel biologic, immunologic and gene therapies designed to promote the control and

eradication of numerous different diseases including cancer, neurodegenerative, inflammatory, infectious, and other diseases. Furthermore, the described detection systems and methods will have broad applications for seamless disease detection and treatment in combined settings.

Other features and advantages of the invention will be apparent from the following detailed description, and from the claims.

DESCRIPTION OF THE DRAWINGS

FIG. 1: Schematic representation of the experimental setup showing the laser source, the light delivery optical fiber, the CCD detector, the optical scanning switch and the imaging plate. In the inset on the upper left corner a top view of the imaging plate depicts the array of the 33 sources on the output glass window.

FIG. 2: a) The optical scanner with the custom designed and manufactured imaging chamber. b) Schematic of the components of the optical scanning device, showing the adjustable input optics with the fiber coupler, the Galvo-controlled mirrors and the telecentric lens used for the production of a flat field at the constant working distance (WD).

FIG. 3: A series of images showing the intrinsic and fluorescence fields used for the calculation of the composite Born field. Each image corresponds to a different source (shown with the black cross in each image). The phantom was a glass tube field with FITC.

FIG. 4: A series of images showing the sources obtained through a homogeneous slab. These images were used for the calculation of the sources positions and co-registered with the white light, also shown for the case of the tube with FITC.

FIG. 5: The FMT structure used for the reconstruction of the measurements. The block diagram represents the whole procedure from the acquisition of the data until the reconstructed value of the fluorochrome concentration is retrieved.

FIG. 6: B) Quantification accuracy of the imaging system in the recovery of the fluorochrome concentration values. A linear response is achieved down to fluorochrome concentrations of 150nM.

FIG. 7: a) The white light image showing the two tubes used for the resolution assessment experiment placed in the imaging chamber at a distance of 0.5 mm. b) Cross sections of two glass tubes containing the same concentration (1200nM) of FITC, placed at the same depth and at varying distances (0.5mm, 0.7mm, 1mm and 1.5mm). Two clear foci were reconstructed.

FIG. 8: Cross sections of two tubes placed at different depths with 1mm horizontal distance and 0.5mm vertical, containing 600nM the upper and 1200nM the lower one.

FIG. 9: Fluorescence reconstruction images of glass tubes containing GFP expressing tumor cells obtained *in vitro* after insertion in the esophagus of nude mice. The two tubes contained 10^5 and 10^6 cells and were inserted at the same depth inside the esophagus. The z coordinate corresponds to the depth of the reconstructed slice.

FIG. 10: a) White light image of a live mouse placed inside the imaging chamber after subcutaneous injection of GFP expressing cells. b) Images of subcutaneously injected GFP expressing cells (under the mammary fat pad) obtained *in vivo*. The number of cells was 10^5. The z coordinate corresponds to the depth of the reconstructed slice.

FIG. 11: a) Schematic of a setup for use with the proposed method in cooperation with a time resolved system employing an ultra-fast laser and an intensified gated CCD camera. B) A close up of the optical scanning device and the imaging chamber. C) A cross section of the proposed imaging chamber.

FIG. 12: Schematic of a setup for combined planar imaging with different projections obtained with the rotation stage. The same setup can be used as a CW or time resolved.

FIG. 13: Schematic of a cylindrical geometry implementation of the methods with the ability to take many projections using a rotation stage. The setup can be used with both CW and pulsed light sources.

DETAILED DESCRIPTION

Optical scanning setup

A schematic of the experimental configuration is shown in Figure 1. An Ar^+ laser emitting maximum of 200mW cw power at 488nm is used for excitation of the fluorescent proteins and it is delivered through a 100μm multimode fiber to the input collimator of the optical scanning head, which substituted the fiber based optical switch of the previous generation system.

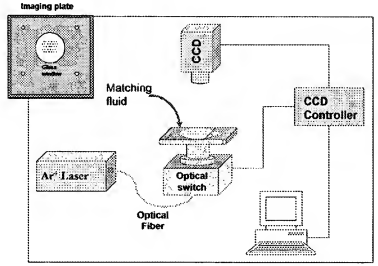

Figure 1

The optical scanner employs two galvanometer controlled mirrors and a scan lens for scanning and focusing the laser beam onto the input window of the chamber. The beam diameter at the focus plane is 300μm. The light delivery is performed with a single fiber from the laser source. A picture of the scanner and the imaging chamber as well as a schematic of its components is shown in Figure 2. With this novel non-contact configuration the disadvantages of the previous fiber based system are eliminated. These include the coupling losses of the fiber switch, the different losses inside each source fiber and the easily damaged fibers, creating thus a more reliable, robust system. Furthermore, the scanning area, the shape as well as the number of sources can be varied (software controlled) and a higher power delivery and a wider tuning range (Visible to NIR) can be achieved. A schematic of a possible array of sources can be seen in the inset of Figure 1. The central source defines the center of the field of view (point (0, 0) in the

FMT code) to better co-register the white light image with the tomographic images taken with the different filters and the final tomographic reconstruction.

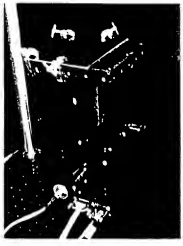

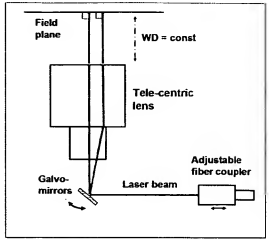

Figure 2

The detection is made with a highly sensitive, cooled CCD camera for reduced dark noise. During acquisition the scanning head is controlled and triggered by the CCD camera's controller so that each obtained image corresponded to a new position of the scanning mirrors (i.e. a different source), thus achieving the proper synchronization of excitation and detection. Each acquisition is composed by N images, one for each source position. This means that the maximum number of data points that this configuration can provide for each set of measurements is Nx512x512 enabling high accurate measurements. However, the number of detectors used for the reconstruction is significantly smaller depending on the field of view defined by the sources array and minimizing the computational time required for the calculations.

Both the phantoms as well as the animal subjects are placed horizontally on the imaging plate and gently compressed with the covering glass. The chamber is then filled with an Intralipid and India ink solution, needed for matching the optical properties and minimizing the index of refraction and diffuse-wave mismatches in the chamber. Breathing of the animals during the *in* vivo studies continues normally through the entire process since the glass window covers the animal body up to the chest living the head and nose well above the liquid surface. The solution consists of 1% intralipid and 2.1% ink, which corresponds to μ_a=1.25cm^{-1} and μ_s'=16.7cm^{-1} for absorption and reduced scattering coefficient respectively.

The light propagation inside the diffusive media was modeled using the modified Diffusion Approximation for high absorbing media derived from the Radiative Transport Equation [20, 21]. Both the intrinsic ~~that is the~~ field generated by the laser excitation light and the fluorescence field which is generated inside the medium due to a fluorochrome at a position $\vec{r}$ are calculated independently and then used to calculate the normalized born field, which is used in the reconstruction algorithm. The born field $U_x(\vec{r}_s, \vec{r}_d)$ at the detectors' position $\vec{r}_d$ due to a source at position $\vec{r}_s$ in a medium with a modified

diffusion coefficient and propagation wavenumbers that account for high absorption is given by:

$$U_e(\vec{r}_s,\vec{r}_d) = S_o \frac{U_{fl}(\vec{r}_s,\vec{r}_d) - \Theta_f U_{inc}(\vec{r}_s,\vec{r}_d)}{U_{inc}(\vec{r}_s,\vec{r}_d)} = \frac{1}{U_o(\vec{r}_s - \vec{r}, k^{\lambda_1})} \int d^3r \cdot U_o(\vec{r}_s - \vec{r}, k^{\lambda_1}) n(\vec{r}) \frac{\upsilon}{D^{\lambda 2}} G(\vec{r}_d - \vec{r}, k^{\lambda_2}) \quad (0.1)$$

where $U_{fl}(\vec{r}_s,\vec{r}_d)$, $U_{inc}(\vec{r}_s,\vec{r}_d)$ are measurements at the emission and excitation wavelengths respectively, $U_{bl}(\vec{r}_s,\vec{r}_d) = \Theta_f U_{inc}(\vec{r}_s,\vec{r}_d)$ is the bleed through signal, Θ_f is the band-pass filter attenuation factor, S_o is a gain term that accounts for instrument gain differences at the excitation (λ_1) and emission (λ_2) wavelengths, $n(\vec{r})$ is the product of the fluorochrome absorption coefficient and fluorescence quantum yield, k^{λ_1} k^{λ_2} are the modified photon wave propagation wavenumbers at λ_1 and λ_2 respectively which account for high absorption, υ is the speed of light into the medium, D^{λ_2} is the modified diffusion coefficient in the presence of high absorption at the λ_2, $U_o(\vec{r}_s - \vec{r}, k^{\lambda_1})$ is a term that describes the established photon field at position $\vec{r}$ into the medium at λ_1 and $G(\vec{r}_d - \vec{r}, k^{\lambda_2})$ is the Green's function solution to the diffusion equation that describes the propagation of the emission photon wave from a fluorochrome at position $\vec{r}$ to the detector given by:

$$G(\vec{r}_d - \vec{r}, k^{\lambda_2}) = \frac{\exp(ik^{\lambda_2}(\vec{r}_d - \vec{r}))}{(\vec{r}_d - \vec{r})} \quad (0.2)$$

The advantage of using the normalized expression are that all the position-dependent contributions are eliminated and more importantly the fact that this field can be calculated even with the presence of the fluorochrome. This means that no background measurements before the administration of the agent are necessary which is very important for *in vivo* studies.

Defining the diffusion length as the rate at which the intensity decays within a medium with reduced scattering coefficient μ_s' as L_d, the diffusion coefficient is given by:

$$D = \mu_a L_d^2, \quad (0.3)$$

where μ_a is the absorption coefficient of the medium. Previously it has been shown that the diffusion length in the presence of high absorption follows the following behavior:

$$\frac{\mu_s'}{\mu_s' + \mu_a} \frac{L_d}{2} \log\left[\frac{L_d + 1}{L_d - 1}\right] = 1 \quad (0.4)$$

From this relation the diffusion coefficient may be extracted resulting in a diffusion coefficient which depends nonlinearly both on the scattering and the absorption properties of the medium. It is convenient to define the modified absorption dependent diffusion coefficient as $D_\alpha \approx 1/3[\mu_s' + \alpha\mu_a]$, where the value of α is extracted from Eqs. (0.3) and (0.4) as:

$$\alpha = \left(\frac{1}{3\mu_a L_d^2} - \frac{\mu_s'}{\mu_a}\right) \quad (0.5)$$

Typical values of α range from 0.2 to 0.5, and in the case of tissue in the visible is in the order of 0.3. It is very important to understand that if the classical descriptions of the diffusion coefficient are used (namely with α=0 or α=1), the diffusion approximation yields inaccurate results. This is the reason why it has been long thought that the diffusion approximation fails in the presence of high absorption. However, as it is taught herein when the modified absorption coefficient is used, the diffusion approximation still holds. To that end, a modified wavenumber must be defined, namely:

$$k^{\lambda} = \sqrt{-\frac{\mu_a^{\lambda}}{D_a^{\lambda}} + \frac{i\omega}{vD_a^{\lambda}}} \tag{0.6}$$

where ω is the modulation frequency (in the CW case ω=0). Herein we discover that based on a modified expression for the diffusion coefficient combined with appropriate changes in the wave propagation wavenumber we can derive Green's function solutions to the diffusion equation that are appropriate for imaging in the visible.

The different optical properties are calculated by fitting the diffused patterns obtained after transmission through a homogeneously scattering slab. The width of the diffused patterns in this case is smaller, thus they are more confined around the central, straight trajectory. This is an effect of the higher absorption and higher scattering of tissue in the visible range. This happens because the photons that are multiply scattered have a higher probability of absorption because of their longer pathlength than the ones that propagate in more straight trajectories. The effect is equivalent to the effect of early temporal gating where only the early arriving and least scattered photons are selectively detected making the distribution of light spatially narrower and the resolution achieved significantly better.

Two types of measurements (shown in figure 3) are acquired during the experiments: fluorescence measurements using band-pass interference filters centered on the fluorescence emission, and intrinsic light measurements obtained by using band-pass interference filter centered on the laser emission. The exposure times can be varied so that dynamic range is maximized. These measurements are used to compose the field $U_c(\vec{r}_s, \vec{r}_d)$.

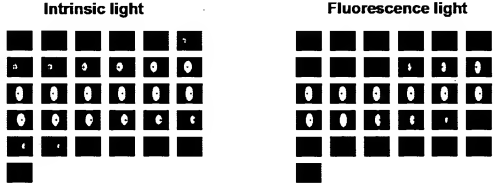

Figure 3

Furthermore, before the acquisition of the FMT images, a white light image is acquired as well as a series of 33 images of the intrinsic light through the homogeneous slab (see

figure 4) so that the location of the sources can be calculated for each individual measurement. This procedure improves the co-registration of white light and tomographic images minimizing any errors.

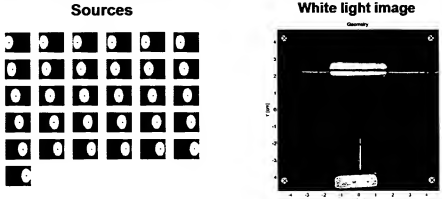

Figure 4

In order to reconstruct the three-dimensional fluorochrome distributions using the composite field measurements, the volume of interest can be segmented into axial (horizontal) layers (e.g. 21) containing a number (e.g. 651) of voxels each. The voxel size depends on the dimension of the field of view and the number of segmentations. The forward model is constructed using the described algorithm and inverted using algebraic reconstruction techniques with positive restriction. Typical inversion times are on the order of 10 min on a 2 GHz Intel Pentium 4 processor. Reconstructed images display the fluorochrome concentration in 3D. The complete FMT procedure can be seen in the block diagram of Figure 5.

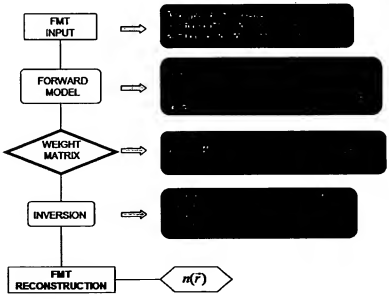

Figure 5

Quantification accuracy

To evaluate the performance of the new system quantification and resolution experiments were performed. The ability of the system to quantify fluorochrome concentrations was assessed by a titration experiment in which thin glass tubes with different (150nM, 300nM, 600nM and 1200nM) concentrations of fluorochrome (Fluorescein Isothiocyanate – FITC) were imaged. They were placed at the center of the field of view and at a depth of 6mm from the input glass window. The acquisition was performed as described in the experimental methods section with a laser power of 100mW. The results are shown in Figure 6 where the reconstructed concentration values are plotted against the real ones.

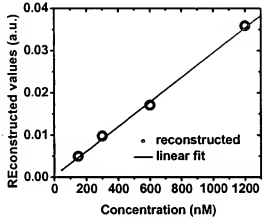

Figure 6

Spatial resolution

The spatial resolution is evaluated by imaging phantoms constructed of two glass tubes containing the same concentration of the fluorochrome place parallel at the center of the field of view, the same depth and at varying separations (0.5mm, 0.7mm, 1mm and 1.5mm). These distances represent the clear gap between the two tubes and not the actual separation of the fluorochrome solution, which is larger. The laser power was 100mW while a linear source array with 31 sources at a distance of approximately 500μm between them was used to increase performance. The reconstructed images are shown in figure 7b, where axial cross sections of the tubes at the center of the field of view are depicted.

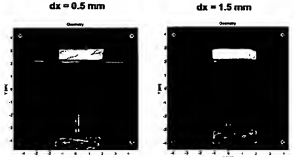

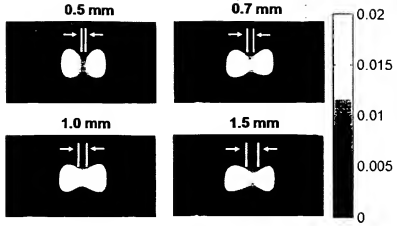

Figure 7

The resolving power of the devise in the z (trans-illumination) direction is shown by imaging a resolution phantom in which two glass tubes with different concentrations (600nM and 1200nM) are placed at a different depth. The horizontal clear gap between the two tubes was 1mm whereas the vertical one was 0.5mm with the higher concentration tube being deeper. Figure 8 shows the reconstructed image where an axial cross section is depicted as above, showing two clear foci at the positions of the tubes. The reconstructed value of the deeper tube was 4.6 times higher.

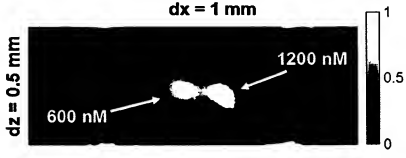

Figure 8

These results show that the spatial resolution achieved using visible wavelengths is higher than the one obtained using NIR light. The corresponding resolution measured with similar experimental and reconstruction configurations with the NIR FMT system was 0.7mm. The higher resolution can be attributed to the higher absorption of visible photons compared to the NIR ones, which eliminates the contribution of the highly diffused photons to the recorded diffused pattern. The result is that only the photons traveling around the central path will be able to reach the detector. Further development of both the experimental setup and the FMT code could boost the resolution to even smaller limits (less than 500μm).

EXAMPLES

1. The new methods make possible the three-dimensional imaging of fluorescent proteins in deep tissues.

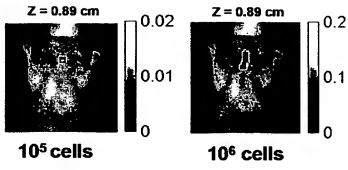

Figure 9

Figure 9 shows an example of such an image capability. Two different numbers of GFP expressing tumor cells were used: 10^5 and 10^6. They were placed inside thin glass tubes and inserted in the esophagus of the animals after they have been sacrificed. The animals were placed inside the imaging chamber, which was then filled with the matching fluid. Imaging was performed using the 33 sources array trans-illuminating the area around the chest of the animal. The goal was to investigate the ability of the system to quantify GFP fluorescence signals originating from deep tissue.

2. The same configuration can be used for whole body imaging of gene expression *in vivo*. An example is given in Figure 10 where sagittal cross sections at different depths of subcutaneously injected GFP expressing cells are presented. The values given represent distances from the bottom of the chamber (from the input window) so the highest value is on the output window.
Development and optimization of the system will allow to image even smaller number of cells bringing the sensitivity limit down to levels comparable to the bioluminescence.

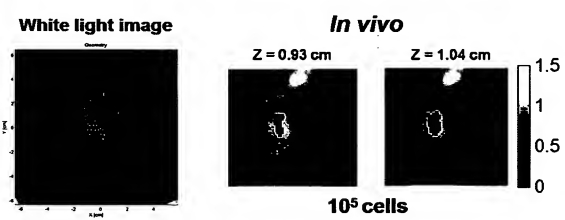

Figure 10

3. The capability of operation in a wide wavelength range and of high power delivery enables the devise to operate with ultra-fast lasers for time resolved and fluorescence lifetime imaging, potentially improving the resolution and the contrast of imaging. The same setup could be implemented in a variety of imaging modalities because of its wide spectral range of operation and capabilities of light delivery, ranging from cw systems in the NIR to time resolved systems with high power ultra-fast pulsed lasers for early time detection and fluorescence lifetime imaging. An example is shown in Figure 11, where a planar imaging geometry is used. The inset is a close up of an example imaging chamber.

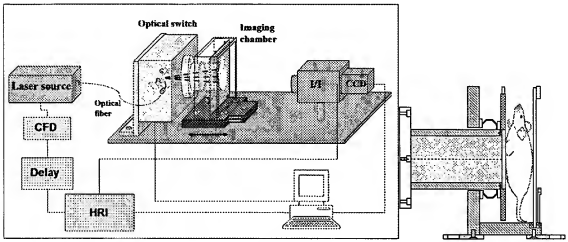

Figure 11

4. The inherent drawback of using visible light for tomographic imaging: the fewer obtained projections, which impair the imaging quality, can be overcome by using an experimental geometry which offers a large number of detection angles. Such a setup is shown schematically in Figure 12 where the planar geometry is combined with a rotation stage. With such a setup high quality 3D imaging can be achieved.

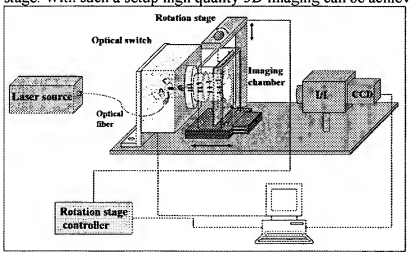

Figure 12

5. The same high quality 3D imaging can be achieved when a cylindrical geometry such the one shown in Figure 13 is used. The advantage is that both the rotation as well as the imaging algorithm is simpler and faster, without imposing drawbacks on the image quality.

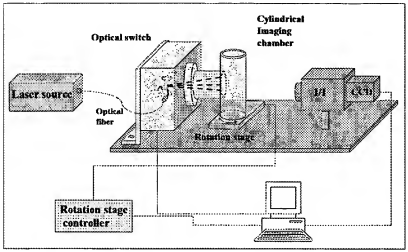

Figure 13

6. The new modality can be used with an improved performance in combination with newly developed fluorescent proteins, namely DsRed and HcRed, because of their emission characteristics in the red region of the spectrum. This would increase the signal detection efficiency because of the larger penetration depth compared with the visible and still maintaining the higher resolution than the NIR light can offer.

7. The new technique can be used for studying tumor growth and monitoring of metastasis formation when used with tumor cells that express fluorescent proteins (like GFP).

8. The new imaging modality can be used with GFP expressing tumor cells and YFP expressing viral cells for the study of gene delivery and gene therapy for specific patient targeted treatment.

9. The new method could be implemented such that they take advantage of novel imaging modalities using newly developed algorithms for imaging arbitrary geometries without the need of the optical properties matching fluids. These algorithms for modeling of light propagation and solving inverse problems could be applied to all of the above geometries and configurations.

CLAIMS

1. A system for optical tomography of a subject using fluorescent proteins within the subject, comprising:

a light source for projecting a plurality of apparent light sources upon the subject and through the subject to intercept the fluorescent proteins and having a wavelength selected to excite visible fluorescent light from the fluorescent proteins, the light source comprising a visible light laser and an optical scanner comprising computer-controlled galvo-controlled mirrors and a telecentric lens;

a cooled CCD camera for receiving visible light from the plurality of apparent light sources and from the fluorescent proteins, and for converting the received visible light into electrical image information; and

an image processor coupled to the cooled CCD camera to process the electrical image information and to provide a tomographic image of the subject and of the fluorescent proteins, wherein the processor includes a diffusion equation processor that uses a modified expression of the diffusion approximation.

ABSTRACT

A method and system for optical tomography using fluorescent proteins includes a light source for projecting visible light upon and through a subject to excite the fluorescent proteins , producing fluorescence light. A light receiver receives the visible light and fluorescence light and generates tomographic images of the subject and of the fluorescent proteins using a modified expression of the diffusion approximation. The modified expression of the diffusion approximation is suitable for high absorption visible light propagation through the diffuse subject.